ELSEVIER

Fusion Engineering and Design 44 (1999) 147–155

Fusion Engineering and Design

# Experiments with ASTERIX and ATLAS

K. Witte[a,*], M. Basko[a], H. Baumhacker[a], A. Böswald[a], K. Eidmann[a], R. Fedosejevs[a], E. Fill[a], V. Kondrashov[a], A. Kendl[a], T. Löwer[a], Y. Li[a], P.X. Lu[a], J. Meyer-ter-Vehn[a], G. Pretzler[a], A. Saemann[a], R. Sigel[a], G. Tsakiris[a], X. Wang[a], A. Benuzzi[b], B. Faral[b], C. Chenais-Popovics[b], M. Koenig[b], H. Merdji[b], D. Batani[c], D. Beretta[c], C. Danson[d], T. Hall[e]

[a] *MPI für Quantenoptik, Hans-Kopfermann-Str. 1, D-85748 Garching, Germany*
[b] *Laboratoire pour Utilisation des Lasers Intenses (LULI), CNRS, Ecole Polytechnique, F-91128 Palaiseau, France*
[c] *Dipartimento di Fisica, Universitá degli Studi di Milano, Via Celoria 16, I-20133 Milan, Italy*
[d] *Rutherford Appleton Laboratory, Chilton, Didcot, Oxfordshire OX11 0QX, UK*
[e] *University of Essex, Wivenhoe Park, Colchester C04 3SQ, UK*

**Abstract**

We report on measurements of the equation-of-state of copper and gold in the multi-ten Megabar range, opacity measurements based on K-shell absorption in aluminium, and X-ray laser studies on a large number of neon-like ions applying the prepulse technique. For these investigations, the one-beam iodine laser facility ASTERIX emitting pulses with energies of up to 1000 J at 1315 nm and of up to 420 J at 438 nm was used. We also give a brief account of experimental and theoretical results referring to the propagation of an ultrashort pulse through underdense hydrogen or nitrogen plasmas and X-ray spectra from an optically field-ionized nitrogen plasma generated either by linearly or elliptically polarized light. For these investigations, 150-fs/200-mJ/800-nm pulses emitted from our titanium:sapphire laser ATLAS were employed. 

*Keywords:* ASTERIX; ATLAS; Copper; Gold

## 1. Introduction

The Laser-Plasma-Group at the Max-Planck-Institut für Quantenoptik at Garching operates two major laser facilities. The one-beam iodine laser ASTERIX as described in detail by Baumhacker et al. [1] emits 450-ps pulses at a repetition rate of 3 shots per hour. At the fundamental wavelength of 1.3 $\mu$m, the pulse energy is up to 1 kJ; at the third harmonic, corresponding to a wavelength of 438 nm, the pulse energy is up to 420 J.

The second facility is a Ti:sapphire laser called ATLAS. It emits 200-mJ/150-fs/790-nm pulses at 10 Hz which can also be frequency doubled

* Corresponding author. Fax: +49 89 32905200.

0920-3796/99/$ - see front matter 
PII:S0920-3796(98)00367-6

with a conversion efficiency of over 40%. By adding a single-shot amplifier to this chain, we have achieved a 150-fs pulse with an energy of almost 1 J and a three-times diffraction limited beam quality. Target experiments with this pulse will be started in April 97. By the beginning of next year, the 10-Hz version of ATLAS will be scaled up to the 1-J level and the single-shot version to the 5-J level. On-target intensities of up to a few times $10^{20}$ W/cm$^2$ are then expected to be available.

## 2. ASTERIX experiments

In the following, brief reports about the experiments recently carried out with the ASTERIX facility will be given. These include EOS measurements using shock waves, opacity measurements, and X-ray lasers.

### 2.1. EOS measurements

By means of the impedance matching technique based on two-step, two-material targets with aluminum as the reference material, we measured the equation-of-state of copper and gold using the labyrinth hohlraum (indirect drive) for the lower pressures and the beam-smoothing phase-zone-plate technique (direct drive) for the larger pressures. The labyrinth hohlraum is designed for single-beam irradiation. Its characteristic feature is an internal cone stopping the incoming laser beam and converting it to primary X-rays such that these cannot hit the target foil. As shown by Löwer and Sigel [2], the shock signals generated with this hohlraum are spatially uniform. They have a rise time of a few ps and a decay time of a few tens of ps indicative of a low preheat level. From measurements with a silicon target, Löwer et al. [3] could further conclude that the temperature increase in the unshocked material due to preheat originating from the driving radiation is below 200 K. Using the phase zone plate technique, we observed shock waves being not completely flat but slightly rounded and a preheat level in the unshocked material somewhat larger than that seen in the hohlraum case but definitely below 0.3 eV. These shortcomings did, however, not impair a correct measurement of the shock front velocity.

Fig. 1 shows two Hugoniot curves 'pressure versus particle velocity' for copper [4] and gold. In the case of copper, our direct and indirect drive measurements agree quite well with former measurements. There are no deviations from the SESAME curve even up to a pressure of 42 Mbar, the largest pressure recorded by us. It is worth noting that with a relatively small laser like ASTERIX the same pressure range can be covered as that realized with nuclear underground explosions requiring by far more expenditures. For gold, the pressures go up to 70 Mbar. There is a slight deviation as to the SESAME curve the origin of which is not yet clarified; this discrepancy needs further investigations.

In addition to these EOS measurements, we also carried out intensive theoretical and experimental studies on the shock wave structure in aluminum and silicon targets which are dealt with in the contribution presented by Basko et al. at this conference [5].

### 2.2. Opacity measurements

The heating of thin foils by means of intense thermal X-rays is a very convenient method to achieve rather homogeneous temperature of a few tens of eV for the purpose of opacity measurements in matter of density of about 10 mg/cm$^3$. Recently Winhart et al. [6] had carried out experiments of this type based on L-shell absorption in aluminum, iron, and holmium in the XUV range at photon energies extending from 70 to 280 eV. In this paper, complementary measurements are presented in the keV photon energy range using the K-shell absorption in aluminum.

An efficient geometry for carrying out these experiments is the set-up as depicted in Fig. 2 [7]. The hohlraum is heated from below by the ASTERIX beam. The other two holes serve as diagnostic holes. The absorber foil is made from a 110-nm thick aluminum layer tamped on both sides by a 50-nm thick carbon layer to reduce the gradients in the aluminum layer upon expansion.

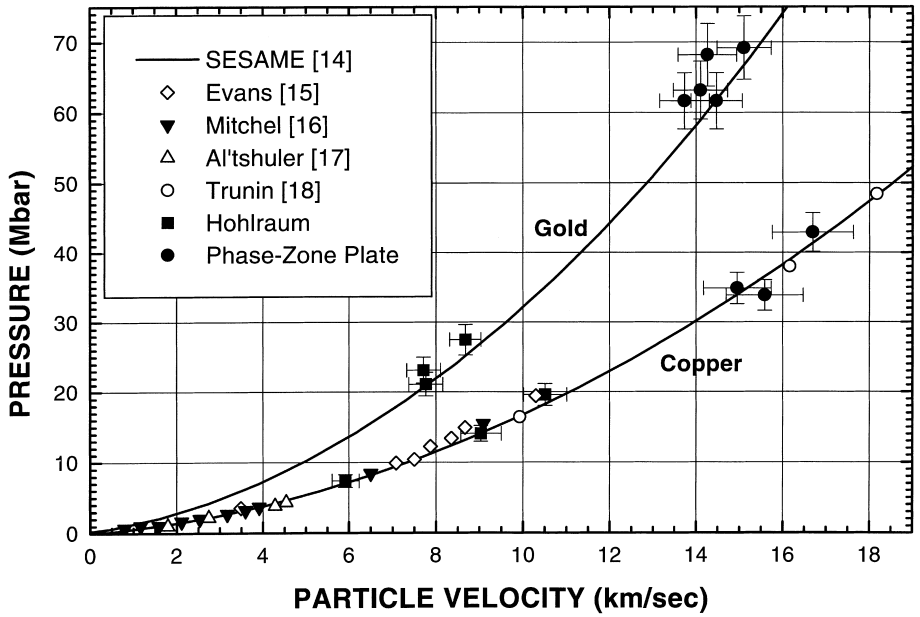


Fig. 1. 'Pressure versus particle velocity' Hugeniot curves for copper and gold. Our experimental results are compared to the SESAME data for copper and gold and also to various previous measurements for copper. The Trunin data [18] were obtained from nuclear underground explosions.

The composite foil is glued to one of the diagnostic holes such that it only covers one half of it leaving the other half open. This made it possible to simultaneously measure the samarium backlighter source spectrum and the absorption spectrum of the aluminum foil in one shot by applying point projection spectroscopy. The spectral resolution is obtained by a flat ammonium dihydrogen phosphate crystal with a resolving power of 1600. The image was recorded on a calibrated KODAK DEF film. The absolute wavelength calibration was provided by prominent samarium lines with an accuracy of 0.4 mÅ. The transmission spectra were calculated by normalizing the absorption spectrum to the source spectrum. The spatial resolution is determined by the backlighter source size and amounts to 100 $\mu$m. Two examples of transmission spectra under different conditions are plotted in Fig. 3. They are dominated by the absorption features due to aluminum ions of charge states from 4+ to 7+. The two different plasma states were realized by using cavities of different sizes and different laser energies. The dotted curves are due to the HULLAC code which assumes LTE. The mean ionization derived from these K-shell absorption spectra coincides well with that found previously from the L-shell absorption spectra [6]. For a precise temperature assignment, the density must be known. Since this dependence is rather weak, a factor-of-three change in the density changes the temperature by not more than 10%. The temperatures given in Fig. 3 are hence rather reliable. It was also found that in very hot cavities non-LTE effects have to be taken into account.

### 2.3. X-ray lasers

The pump energy requirement of X-ray lasers can be considerably reduced by the prepulse technique [8]. We investigated this scheme with our ASTERIX facility in an extensive series of experiments. The energy of the prepulse which preceded the main pulse by 5 ns was varied from 0.5 to 1.5% of that of the main pulse. Both pulses are focused onto the plane target surface in the form of a line focus 3 cm long and $\sim$150 $\mu$m wide by means of a six-element cylindrical lens array.

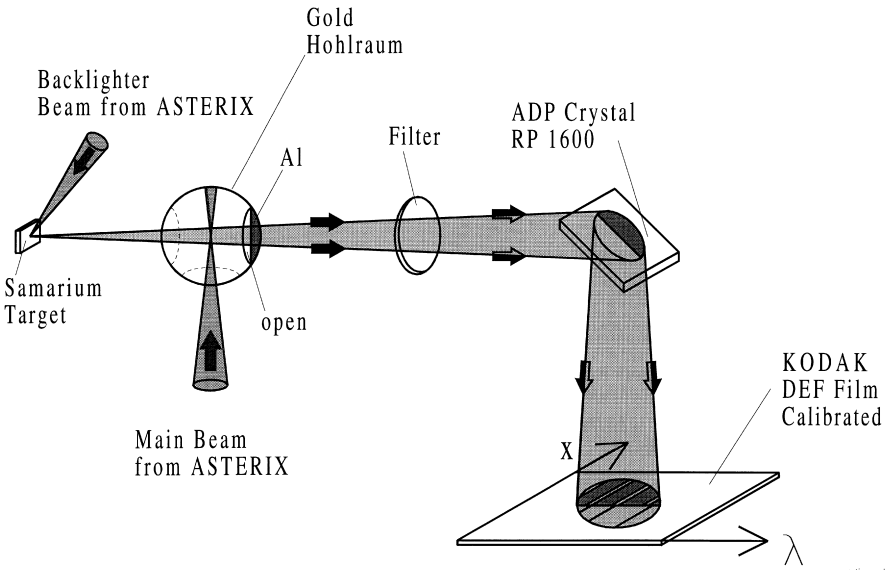


Fig. 2. Scheme of the experimental set-up.

Due to the time delay between the prepulse and the main pulse, the preplasma can expand so that on the arrival of the main pulse its density gradient normal to the target surface is considerably lower than that occurring when the plasma is generated by a single strong pulse. The role of the main pulse is then just to heat the electrons without degrading the plasma homogeneity. Hence the deflection experienced by the X-ray beam when propagating through this plasma is reduced and the gain region is enlarged. This combined action creates a more uniform, larger scale length plasma, allowing the X-ray beam to completely remain within the gain region and not to be forced to leave it prematurely.

With the experimental arrangement as briefly described above, nine new Ne-like lines could be made to lase. With the exception of $Ga^{21+}$, their intensities are plotted versus wavelength in Fig. 4 starting with manganese, chromium, and vana-

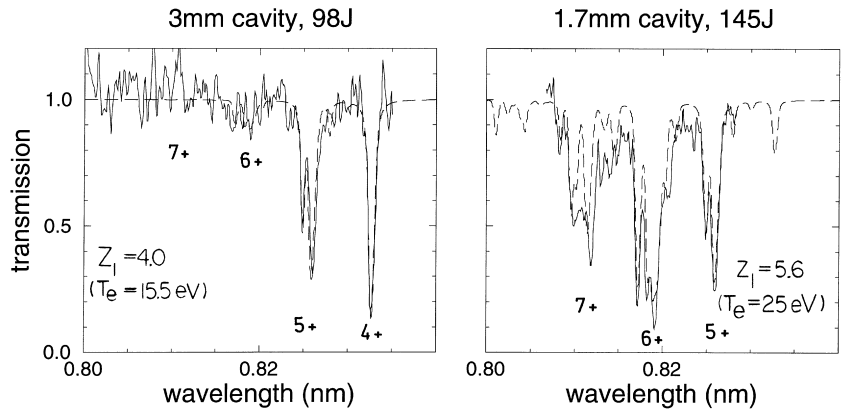


Fig. 3. Measured (solid line) and calculated (HULLAC code, dotted line) transmission spectra. $Z_I$ is the mean ionization and $T_e$ the electron temperature. The densities assumed are (left) 3 mg/cm$^3$ and (right) 10 mg/cm$^3$.

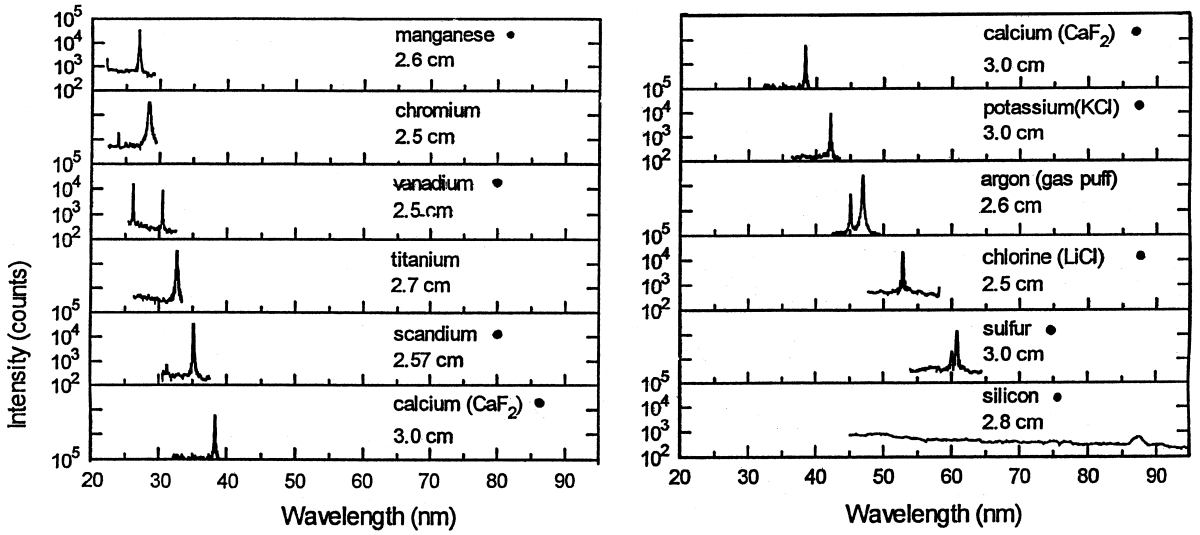


Fig. 4. Relative intensity vs. wavelength of Ne-like ions lasing in the region extending from SXR to XUV. The new lines are marked with a dot. For each element the target length is given in cm.

dium on the short-wavelength side and ending with chlorine, sulfur, and silicon on the long-wavelength side in the XUV range. The new lines are marked with a dot.

By optimizing the prepulse level, the efficiency of all the neon-like X-ray lasers which we looked at for this purpose could be considerably improved. As a prominent example, we mention sulfur which we could make to lase with only 20 J of pump energy at a prepulse energy of 0.4 J [9]. Lasing was checked by looking at the near field pattern of the radiation emitted from one end of the plasma column. This pattern was imaged onto a CCD camera in front of which a 5000 lines/mm transmission grating with a 50-$\mu$m wide slit was placed. The spatial resolution of this device is perpendicular to the target surface, the spectral resolution parallel to the target surface. In Fig. 5, a round spot at 61 nm clearly contrasted with the plasma background radiation and hence indicating strong laser emission can be seen accompanied by two diffraction spots due to the 4-$\mu$m support structure of the grating. In a future series of measurements, we will employ the prepulse scheme in our ATLAS laser using its sub-ps pulses for the main beam. Due to the transient nature of

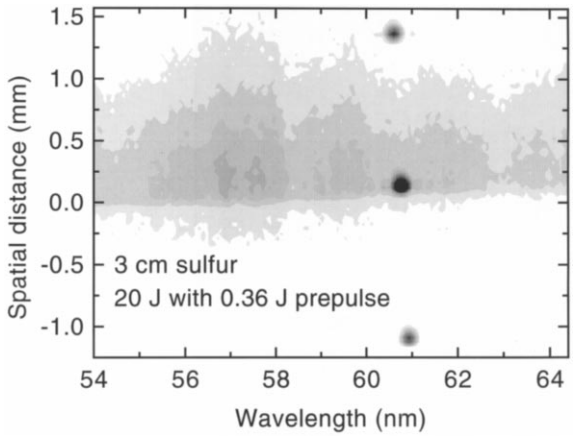


Fig. 5. Record of a spatially resolved spectrum from a 3-cm long sulfur target.

the excitation processes, it is expected that the pump energy requirement is further reduced to the level of not more than a few Joules.

## 3. ATLAS experiments

The experiments we are currently carrying out on our 150-fs-ATLAS laser system encompass harmonics from solid surfaces, energy transport

in and spectroscopy of fs-plasmas using multi-layered targets, fs-pulse propagation through an underdense plasma, and optical field ionization. Only the latter two experiments will be reported in the following since the first two are only at the beginning.

### *3.1. Femtosecond-pulse propagation through an underdense plasma*

Gas puff targets provide one of the simplest forms of underdense media. Upon penetrating through the gas cloud the laser pulse ionizes the atoms or molecules crossing its way. The predominant ionization mechanism is tunnel ionization which under our conditions occurs instantaneously. Since the peak intensity of the pulse is close to $10^{18}$ W/cm$^2$ the ionization takes place far in its leading edge so that the main body of the pulse sees a gas already ionized. When propagating through this plasma the laser pulse is subject to three processes modifying its transverse profile in a subtle way: relativistic self-focusing, diffraction, and ionization refraction. Given a bell-shaped intensity profile, the latter effect defocuses the laser beam since the refractive index of the plasma, $\eta$, obeys the relation $(1-\eta) \propto n_e$ where $n_e$ is the electron density which is proportional to the pulse intensity. This means that where the intensity is high the refractive index, $\eta$, is low and vice versa. Hence a bell-shaped profile leads to beam spreading besides that due to diffraction. This situation usually occurs in gases made up of atoms with medium to large Z-numbers when the pulse intensity is not strong enough to generate a plasma with a homogeneous electron density by fully stripping the ions being located in the beam path. In a completely ionized medium, however, ionization refraction plays no role due to the absence of transverse electron density gradients. Because in hydrogen only one electron has to be removed per atom it is a gas where this situation can be realized at modest intensities of about $10^{14}$ W/cm$^2$.

In order to analyze the laser pulse-gas interaction as thoroughly as possible we applied various different diagnostic methods: time-resolved shadowgraphy of the focal volume using the 2-$\omega$ probe pulse which crosses the 1-$\omega$ pulse at right angle and whose delay can be varied, images of the 1-$\omega$ pulse in a plane perpendicular to the beam axis 250 $\mu$m beyond vacuum focus, self-scattered time-integrated images of the 1-$\omega$ radiation at 90° to the main beam axis, time-integrated images of the plasma using its 2-$\omega$ emission, Raman scattering, and hard X-ray measurements. Examples of the first two diagnostic methods are shown in Fig. 6. The electron densities for $N_2$ and $H_2$ are about equal. The shadowgraphy images are taken 1.3 ps after the leading edge of the pulse reaches the vacuum focus. In nitrogen, ionization defocusing clearly dominates. In the fully ionized hydrogen, however, only self-focusing and diffraction remain as competing processes whereby self-focusing appears to dominate over diffraction. The transmitted images further support this interpretation. Ideally, there should be only one self-focusing channel in hydrogen. We attribute the beam break-up into two spots to the intensity profile of the focused 1-$\omega$ pulse which exhibited two clearly distinguishable peaks. Only in the case of hydrogen did we observe strong X-ray signals. In Fig. 7, they are plotted versus electron density $n_e$ normalized to the critical electron density $n_C = 1.75 \times 10^{21}/\text{cm}^3$ as calculated for a pulse carrier wavelength of 800 nm. At constant laser power, $P_L$, the transition to the regime dominated by self-focusing can be achieved by increasing the gas density and hence also the electron density. The threshold value, $n_S$, corresponding to this transition is plotted as a vertical dotted line in Fig. 7, whereby $n_S$ is determined from the well-known relation [10] $P_C/\text{GW} = P_L/\text{GW} = 16 n_C/n_S$ with $P_L = 300$ GW as the power used in these hydrogen experiments. The horizontal dashed line corresponds to the detection limit. In hydrogen, there should be no significant X-ray production in the plasma itself. However, due to relativistic self-focusing fast electrons are generated [11] which when hitting the rim of the gas nozzle cause the production of hard X-rays. The most interesting result is that the onset of hard X-ray emission is consistent with the threshold for the onset for relativistic self-focusing as predicted by Pukhov and Meyer-ter-Vehn [11].

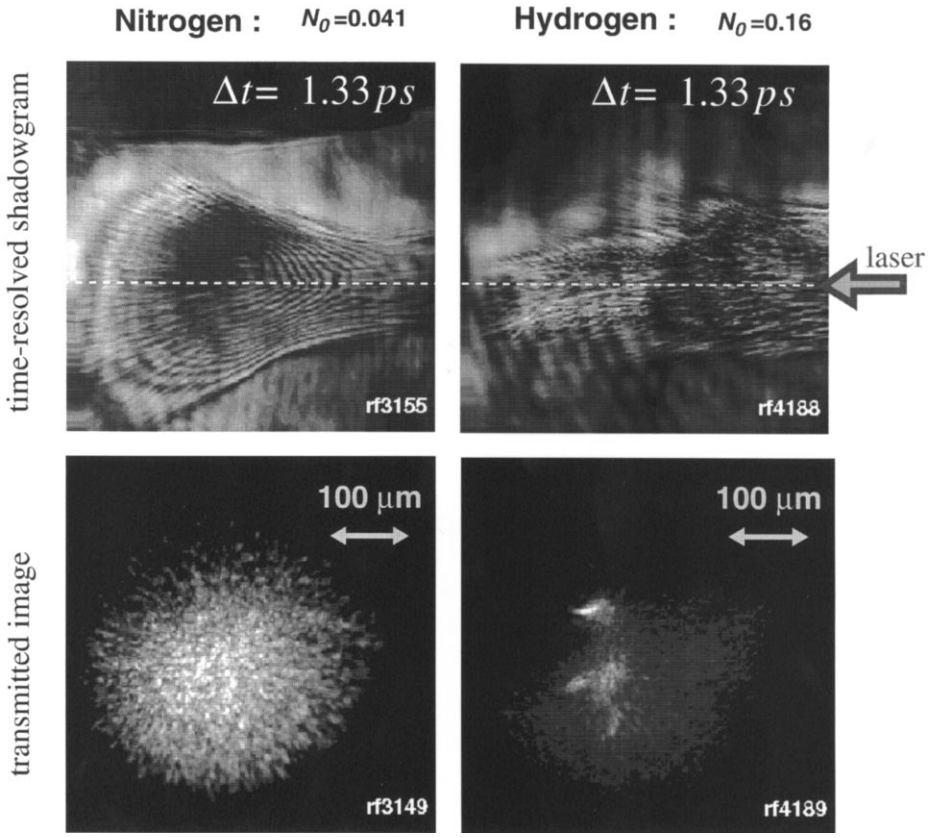


Fig. 6. Shadowgrams (upper half) taken with the 2-$\omega$ probe pulse and transmitted images (lower half) 250 $\mu$m past focus showing the interaction of the 0.3 TW Ti:sapphire pulse with 500-$\mu$m nitrogen and hydrogen gas jet targets.

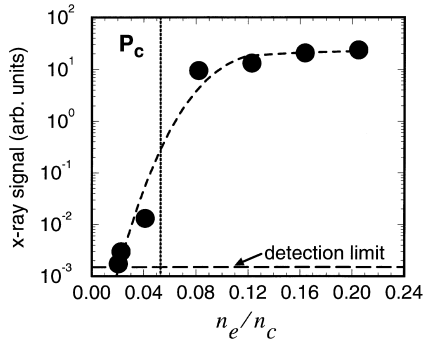


Fig. 7. Hard X-ray emission (> 12 keV) vs. normalized electron density. The vertical dashed line marks the transition to the region dominated by self-focusing.

### 3.2. Optical field ionization (OFI)

We compare X-ray spectra from optical-field ionized plasmas which were generated either by linearly or elliptically polarized light [12]. It has been theoretically predicted by Corkum et al. [13] that there should be a considerable difference between these two cases as to the electron temperature. We demonstrate that this difference also manifests itself in different intensities of X-ray lines emitted from these plasmas.

The experimental set-up for studying this effect is rather simple. The ATLAS pulse is focused into a cell containing nitrogen at pressures around 1 mbar. At this level, masking effects such as clustering and electron heating by inverse Bremsstrahlung or Raman scattering are avoided. The X-ray spectra from the OFI plasmas are recorded by a spectrometer consisting of a transmission grating and a backside illuminated CCD camera. The pulse intensity in the focal region was set to $3 \times 10^{16}$ W/cm$^2$. At this intensity level, theory predicts the occurrence of helium-like ni-

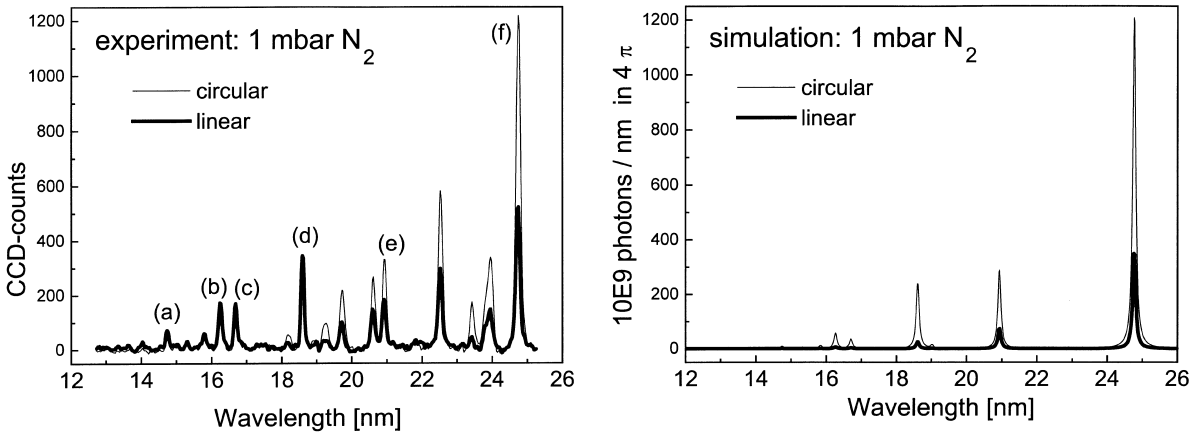


Fig. 8. (Left) Soft X-ray spectra from nitrogen. $N^{4+}$-lines: (a) 2s-5p, (b) 2s-4p, (c) 2p-5d, (d) 2p-4d, (e) 2s-3p, (f) 2p-3d. The other lines are due to $N^{3+}$. (Right) Simulated time-integrated soft X-ray spectra for $N^{4+}$.

trogen. As expected, the spectra exhibit lines emitted from lithium-like and beryllium-like nitrogen ions. In the left half of Fig. 8, a nitrogen spectrum containing lines from $N^{3+}$ and $N^{4+}$ is shown. The effect of the ellipticity of the laser pulse is quite significant. Most lines, e.g. 2p-3d and 2s-3p in $N^{4+}$, generated with elliptically polarized light are much stronger than those generated with linearly polarized light. This result is a first demonstration of Corkum's conjecture [13] and may have important consequences for OFI X-ray lasers using recombination or electron collisional pumping [14–17]. There are, however, some unexpected anomalies for lines which originate from levels with higher principal quantum numbers such as 2p-4d and 2p-5d in $N^{4+}$, where a behaviour opposite to that just mentioned is observed. A clarification of this effect is expected from future investigations.

Simulations of the experimental spectra were carried out for helium and nitrogen using a collisional radiative code. It calculates time-dependent level populations and the spectra emitted from the plasma. The initial conditions for the electron temperature, electron density, and ionic abundances are obtained by integrating the rates of the various ionization stages over the pulse width. Electron temperatures of 15 and 85 eV were found for nitrogen in case of linear and elliptical polarization, respectively. As can be seen from the right half of Fig. 8, the simulations which contain no adjustable parameters predict a ratio of the Li-like 2p-3d lines in $N^{4+}$ approximately equal to that experimentally observed. However, for transitions originating from higher principal quantum numbers like the 2p-4d transitions in $N^{4+}$ the code simulations fail. A clarification of this effect is also expected from further investigations.

## Acknowledgements

This research was supported in part by the Commission of the European Union in the framework of the association Euratom/Max-Planck-Institut für Plasmaphysik and also in part by the EU Human Capital and Mobility program under Contract No. ERB-CH-CT920006.

## References

[1] H. Baumhacker, G. Brederlow, E. Fill, R. Volk, S. Witkowski, K. Witte, Appl. Phys. B61 (1995) 325–332.

[2] Th. Löwer, R. Sigel, Uniform shock waves driven by thermal radiation from laser heated cavities, APS Conference on Shock Compression of Condensed Matter, American Institute of Physics Conf. Proc., Seattle/USA, 370 (1995) 1261–1264.

[3] Th. Löwer, V.N. Kondrashov, M. Basko, A. Kendl, J. Meyer-ter-Vehn, R. Sigel, Reflectivity and optical brightness of laser-induced shocks in silicon, accepted for publication in Phys. Rev. Lett., May 1998.

[4] A. Benuzzi, Th. Löwer, M. Koenig, et al., Phys. Rev. E 54 (1996) 2162–2165.
[5] Th. Löwer, M. Basko, V. Kondrashov, R. Sigel, A. Kendl, J. Meyer-ter-Vehn, Optical probing of laser-induced shock waves in aluminum and silicon, Proceedings of the IAEA Technical Committee Meeting on Drivers and Ignition Facilities for Inertial Fusion, Osaka, Japan, March 10–14, 1997.
[6] G. Winhart, K. Eidmann, C.A. Iglesias, A. Bar-Shalom, Phys. Rev. E 53 (1996) R1332–R1335.
[7] H. Merdji, K. Eidmann, C. Chenais-Popovich, G. Winhart, J.C. Gauthier, A. Mirone, A. Iglesias, K-Shell spectroscopy of radiatively heated aluminum, Paper presented at the 7th International Workshop on 'Radiative Properties in Hot Dense Gases', 31 Oct. to 4 Nov. 1996 in Santa Barbara, CA/USA; also submitted for publication to J. Quant. Spectr. Radiat. Transfer (JSQRT).
[8] Y. Li, G. Pretzler, P. Lu, E.E. Fill, J. Nilsen, Phys. Plasmas 4 (1997) 479–489.
[9] Y. Li, P. Lu, G. Pretzler, E.E. Fill, Opt. Commun. 133 (1997) 196–200.
[10] G.Z. Sun, E. Ott, Y.C. Lee, P. Guzdar, Phys. Fluids 30 (1987) 526–530.
[11] A. Pukhov, J. Meyer-ter-Vehn, Phys. Rev. Lett. 76 (1996) 3975–3978.
[12] G. Pretzler, E.E. Fill, Opt. Lett. 22 (10) (1997) 733–735.
[13] P.B. Corkum, N.H. Burnett, F. Brunel, Phys. Rev. Lett. 62 (1989) 1259–1262.
[14] T4 Group LANL, SESAME Report on the Los Alamos Equation-of-State Library, LANL Report No. LALP-83-4, 1983.
[15] A. Evans, N. Freeman, S. Rothman, Feasibility of Hugoniot EOS measurements on HELEN, Paper presented at the 23rd European Conference on Laser Interaction with Matter (ECLIM), 19–23 September 1994 in Oxford/UK, Institute of Physics Conference Series No. 140, 1995, pp. 235–238.
[16] A.C. Mitchell, W.J. Nellis, W.J. Moriarty, et al., J. Appl. Phys. 69 (1991) 2981–2986.
[17] L.V. Alt'shuler, S.B. Kormer, A. Bakanova, R. Trunin, Sov. Phys. JETP 11 (1960) 573–579.
[18] R.F. Trunin, Phys. Uspekhi 37 (1994) 1123–1145.